Available online at www.sciencedirect.com
SCIENCE DIRECT®
International Journal of Thermal Sciences 44 (2005) 349–356
International Journal of Thermal Sciences
www.elsevier.com/locate/ijts

CFD turbulent modelling of jet impingement and its validation by particle image velocimetry and mass transfer measurements

M. Angioletti [a], E. Nino [a], G. Ruocco [b,*]

[a] *DIFA, Università degli Studi della Basilicata, Campus Macchia Romana, 85100 Potenza, Italy*
[b] *DITEC, Università degli Studi della Basilicata, Campus Macchia Romana, 85100 Potenza, Italy*

Received 10 October 2004; received in revised form 18 October 2004; accepted 3 November 2004

Abstract

Heat transfer by initially laminar and transitional submerged, unconfined gaseous jet impingement on a plane target is analyzed numerically and additionally interpreted with the help of associated measurements. Qualitative and quantitative comparisons for three different regimes, in the transitional regime (initially laminar or low turbulence impinging jets) between $Re = 1000$ and 4000 are presented.

A combined experimental approach has first been exploited. By using a Particle Image Velocimetry (PIV), instantaneous flow field data have been extracted and properly averaged to focus on flow field modifications at free-jet interface and along its way to impact and dispersion. Furthermore, a dimensionless local heat transfer *Nu* is locally assessed by micrometric measurements of ablation depth of a naphthalene film.

Finally, the subject configuration has been modelled by a commercial CFD code, allowing to assess its validity. Three turbulence models have been enforced in the present paper, and complete velocity maps and local *Nu* distributions are presented and compared to the averaged or instantaneous experimental flow field and heat transfer data, helping ascertain on the relative merits of the adopted models.

Keywords: Jet impingement; Local heat transfer; PIV visualization; CFD modelling

1. Introduction

Jet impingement (JI) heat transfer is the subject of a vast research activity, as reviewed in [1,2]. The JI concept consists in directing a jet flow from a nozzle of a given configuration to a target plane or modified surface (Fig. 1), and is employed in many important applications as diffusive or convective heat transfer processes, where an accurate assessment or control of the local heat transfer distribution is required. The available studies have been mainly focused in so far on turbulent JI, as initially laminar or transitional jets being left relatively unexplored. The experimental characterization at low-turbulence values of the inlet jet Reynolds number is rather critical as the induced flow field is very responsive to transient fluid structures being formed at interface with quiescent medium, strongly affecting local heat transfer at the target as briefly recalled in the following.

The limit at which the circular unconfined jet becomes a transition or semi-turbulent one is for $Re = 1000$ [2], based on nozzle diameter. This limit identifies a peculiar regime in which the jet, although initially laminar at the nozzle exit, evolves into a non-isotropic jet, on its way to impact. Four regions are typically formed by the impinging jet, as depicted in Fig. 1, and are referred to in this paper. The free jet region (where the jet axial velocity is almost constant to its nominal value) interacts with the quiescent air, generating a train of macro-structures. Below this two region, the jet gradually decelerates to impact in the stagnation region, where almost all kinetic energy is transformed into a static pressure rise. Following impact, the jet flow is redirected along the target surface in the wall jet region, comprising the boundary layer, first resuming most of its pristine velocity, then relaxing upon expansion, and eventually separating and recirculating.

* Corresponding author.
E-mail address: ruocco@unibas.it (G. Ruocco).

1290-0729/$ – see front matter
doi:10.1016/j.ijthermalsci.2004.11.010

Nomenclature

a	thermal diffusivity	$m^2 \cdot s^{-1}$	
d	nozzle diameter	m	
H	nozzle height	m	
k	turbulence kinetic energy	$J \cdot kg^{-1}$	
Nu	Nusselt number, Eq. (1)		
p	pressure	Pa	
Pr	Prandtl number, Eq. (1)		
r	radius, radial position	m	
Re	Reynolds number		
Sc	Schmidt number, Eq. (1)		
Sh	Sherwood number, Eq. (1)		
T	Temperature	K	
u, v	velocity components	$m \cdot s^{-1}$	
V	velocity magnitude	$m \cdot s^{-1}$	
x	axial position	m	

Greek symbols

ε	turbulent dissipation rate	$m^2 \cdot s^{-3}$
θ	time	s
ν	kinetic viscosity	$m^2 \cdot s^{-1}$
ω	specific dissipation rate	s^{-1}

Subscripts

av	average
t	turbulent

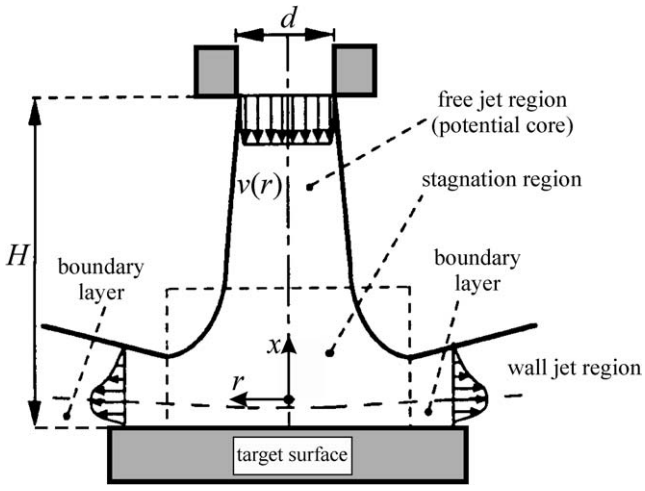

Fig. 1. Characteristic regions in submerged, unconfined JI.

The heat transfer capability of such a stream is thoroughly described in the available literature as far as the stagnation (nominal point of impact) is concerned, depending on the jet core length. But in these laminar or transitional configuration, as recently confirmed by an experimental investigation by the same authors [3], JI features some periodic turbulent macro-structures which interfere with otherwise laminar boundary layer formed on the impinged plate. Starting on the margin of the stagnation region and through the wall jet region onset, local heat transfer rate maxima are therefore detected due to the influence of macro-structures formed by the jet on its way to impact on the stagnation/wall boundary layer. Downwind flow separation and recirculation may also contribute to the additional departure from heat transfer non-monotone progress.

At this point, it is useful that attention be turned to the associated computational description of the transitional JI, to speculate on CFD ability in quantifying this peculiar thermal-fluid pattern. Careful CFD is an important tool when analysis and prediction of heat transfer is demanded. This paper employs the commercial code FLUENT™ and seeks for its validation with the associated measurements: Particle Image Velocimetry (PIV) is used in this context for the first time to qualitatively compare with the computational results for each characteristic regions formed upon JI, and for each of the available turbulence models. In addition, the heat transfer to the target surface is quantified by a mass transfer technique and compared again with the numerical results.

The transitional range $Re = 1000$–4000 is exploited, while no such data are given in the reference review by Polat et al. [4], as well as in the most recent numerical works at hand [5,6]. To isolate the CFD performance dependance on the *Re* regime, only one value of jet height has been used.

2. Experimental set-up

The ducting employed is depicted in Fig. 2. Air is drawn from the outdoor, stored in an adiabatic compressor plenum (not shown), and ducted through a flow meter to a hose ending with a smaller secondary plenum. The regularity of the airflow and uniformity of temperature has been ensured by a regulating valve and by carefully checking a related thermocouple throughout the tests. The secondary plenum is levelled and suspended above the test plate by a micrometer static guide. The air is then blown through an attached 10 mm TSI calibrated converging nozzle, which ensures an essentially uniform initial velocity profile $V(r) = V_{av}$ and low turbulence, and impinges on the target test plate. The JI system is mounted within a controlled test room, where stale air is withdrawn by a blower and ducted to the outdoor.

The PIV system (Fig. 3) has been employed to analyze the instantaneous behavior of the velocity field, using a measurement grid of 116×93 (the reader is referred to details published elsewhere [3], as mentioned earlier). The measurements are then time-averaged properly (see [7]).

The well-known mass/heat transfer analogy has been simultaneously enforced to characterize the local heat transfer. To this end, naphthalene films have been exposed to ablation by the jet to produce modified surfaces, which can then

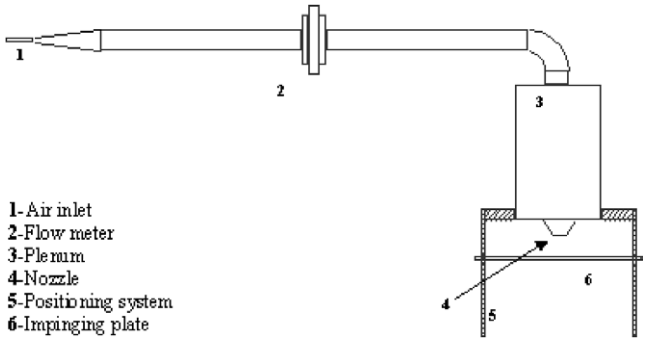

Fig. 2. System layout of JI generation.

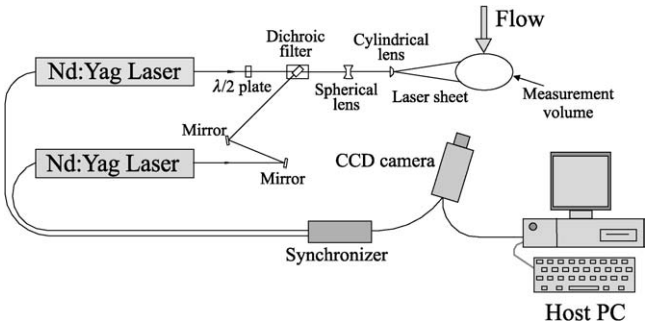

Fig. 3. PIV set-up and system components.

be measured by a micrometric digital probe. Then, based on ablated depth values, the distribution of local Sherwood number can be inferred, and finally the related Nusselt number distribution is found [3]:

$$Nu(r) = \left(\frac{Pr}{Sc}\right)^{0.4} Sh(r) \tag{1}$$

3. Computational approach

The cooling impinging jet discharges vertically (see Fig. 1) from an adiabatic feed tube into an unconfined space, limited by a heated solid substrate, with a uniform outlet velocity profile (only half section of the domain is considered due to the geometry and thermal symmetries). The following assumptions are adopted:

(1) The flow is axisymmetric and incompressible with constant properties.
(2) The viscous heat dissipation is neglected.
(3) A constant temperature condition is applied to the impinged plate (no-slip is considered).

With reference to the previous statements, the standard RANS and energy equations are enforced:

Continuity:

$$\frac{\partial u}{\partial x} + \frac{\partial v}{\partial r} + \frac{v}{r} = 0 \tag{2}$$

Momentum in the axial direction:

$$\frac{\partial u}{\partial \theta} + u\frac{\partial u}{\partial x} + v\frac{\partial u}{\partial r} = -\frac{\partial p}{\partial x} + \frac{\partial}{\partial x}\left[2(\nu+\nu_t)\frac{\partial u}{\partial x}\right] + \frac{1}{r}\frac{\partial}{\partial r}\left[(\nu+\nu_t)r\left(\frac{\partial u}{\partial r} + \frac{\partial v}{\partial x}\right)\right] \tag{3}$$

Momentum in the radial direction:

$$\frac{\partial v}{\partial \theta} + u\frac{\partial v}{\partial x} + v\frac{\partial v}{\partial r} = -\frac{\partial p}{\partial r} + \frac{\partial}{\partial x}\left[(\nu+\nu_t)\left(\frac{\partial u}{\partial r} + \frac{\partial v}{\partial x}\right)\right] + \frac{1}{r}\frac{\partial}{\partial r}\left[2(\nu+\nu_t)r\frac{\partial v}{\partial r}\right] - (\nu+\nu_t)\frac{v}{r^2} \tag{4}$$

Energy:

$$\frac{\partial T}{\partial \theta} + u\frac{\partial T}{\partial x} + v\frac{\partial T}{\partial r} = \frac{\partial}{\partial x}\left[(a+a_t)\frac{\partial T}{\partial x}\right] + \frac{1}{r}\frac{\partial}{\partial r}\left[(a+a_t)r\frac{\partial T}{\partial r}\right] \tag{5}$$

The closure relationships for ν_t can be assumed from the chosen turbulence model, in this case the k–ε *Re*–Normalized Group (k–ε RNG) or the k–ω Shear Stress Transport (k–ω SST), or by reconstructing the Reynolds stresses by the use of the Reynolds Stress Model (RSM). Being their treatment beyond the scope of the present work, the Reader is referred to the FLUENT^{TM} User's guide [8] for their complete formulation.

The working fluid is air, which is injected at atmospheric pressure and isothermal with the surround air ($T = 298$ K). The target surface is kept at 308 K. The distribution inlet velocity of jet is assumed as the one measured by the PIV measurements. A test on the independency of the flow field on the initial turbulence intensity has been also performed, and a 0-value has been used throughout the computations. This is found consistent to the fact that a calibrated nozzle was used in the experiments.

The effect of the different values of domain radial and axial lengths has first been monitored, to enforce the boundary condition of undisturbed flow. A value of 10 nozzle diameters was finally chosen, as radial and axial lengths. A stretched grid of 86×81 has been employed, as presented in Fig. 4, for all computations, to resolve the velocity and pressure gradients in the boundary layer, induced by the impingement and redirection of flow. Minimum radial and axial sizes of cell have been set equal to 5×10^{-4} m. A grid-independence positive check has also been performed on a 170×160 grid. Time steps have been kept consistently small to ensure stability, typically 2×10^{-5} to 1×10^{-4} s.

A segregated solver with 2nd order unsteady implicit formulation has been employed throughout, as the standard under-relaxation parameters. The residuals were kept set 1×10^{-3} for all variables, except for temperature (1×10^{-6}). Steady-state elapsed time was assumed 10 s for all runs, with

execution times ranging from 72 to 150 h on a Pentium IV (WindowsXP OS, 2.0 GHz, 1 GB RAM).

Once the thermal field is obtained, it can be rendered dimensionless based on the target-inlet temperature difference, whereas the x-coordinate is rendered dimensionless based on nozzle diameter. Hence, a local Nusselt number can be evaluated at the target surface, by using a 4-point Lagrangian interpolation of dimensionless temperature derivative calculated at domains interface:

$$Nu(r) = -\left(\frac{\partial T'}{\partial x'}\right)_{x'=0} \tag{6}$$

4. Results

The three turbulence models mentioned earlier have been employed to simulate the flow and temperature fields of configurations that were explored by the associate experiments. In the following Figs. 5 to 10, the related flow fields are qualitatively compared with the PIV visualizations, by coupling the filled iso-areas plots of velocity magnitude in the $r - x$ section (with respect to dimensionless height H/d and position r/d). The results generated are qualitatively acceptable, with reference to the general appearance of the flow field. Let us briefly comment on the appearance of the flow field, for the two regimes at hand ($Re = 1000$ and 4000), with reference to regions presented in Fig. 1.

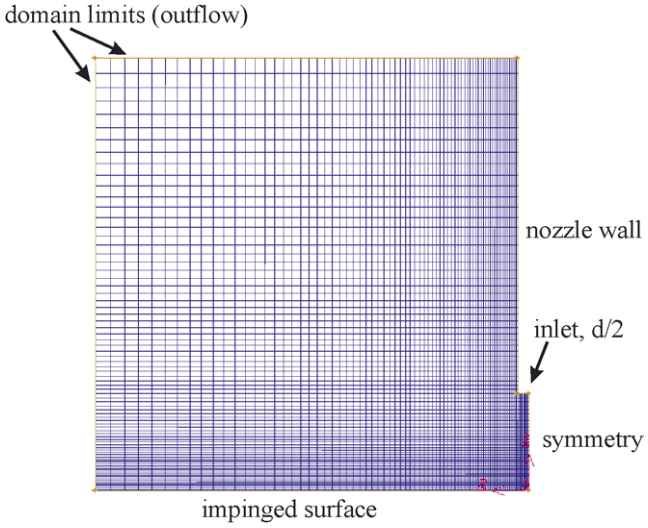

Fig. 4. Computational domain.

When *Re* is set to 1000 (Figs. 5, 7 and 9), it is seen that k–ω SST (Fig. 5) responds more properly reducing the expansion of the developing core region. In addition, the stagnation region is nicely configured, but the boundary layer in the wall jet region is too much constrained along the target. The k–ε RNG (Fig. 7) and RSM (Fig. 9) simulations defect in the core region, as they show a clipped core, or a dissolved region, respectively. The k–ε RNG (Fig. 7) appears more consistent instead in the wall jet region where adequately shows the typical impingement re-acceleration and separation behaviors.

When *Re* increases up to 4000 (Figs. 6, 8 and 10), model performances appear quite reversed. Both k–ε RNG and RSM models perform nicely in all jet impingement characteristic regions, while the k–ω model presents inhomogeneous sub-regions at the end of the jet core, starting deceleration to stagnation.

The different performances of the JI turbulence modelling in FLUENT^{TM} are commented in the following. In Fig. 11 the prediction by the k–ω model (right side) is compared with the correspondent experimental data (left side), by superimposing the filled areas to iso-contour lines. It is seen that k–ω SST gives out an instantaneous representation of the flow field: the alternate reductions and expansions of the core region are due to the joint action of entrainment and slip flow over the stagnation region, and to the toroidal vortex train, already alluded to in [3]. The PIV technique, though instantaneous itself, has been enforced instead in this work by time-averaging the signal in the measurement volume, therefore such pulsations cannot be evidenced.

In a fully-turbulent condition ($Re = 4000$) instead, the contingent non-homogeneous vortex regions (Fig. 6, right

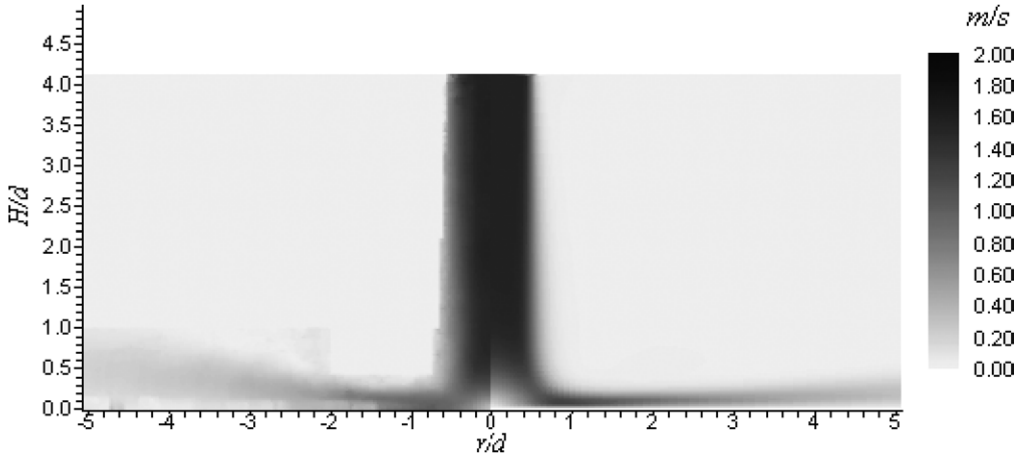

Fig. 5. Comparative PIV (left)/FLUENT^{TM} (right) shaded plots of V. k–ω turbulence model for $H/d = 4.5$: $Re = 1000$.

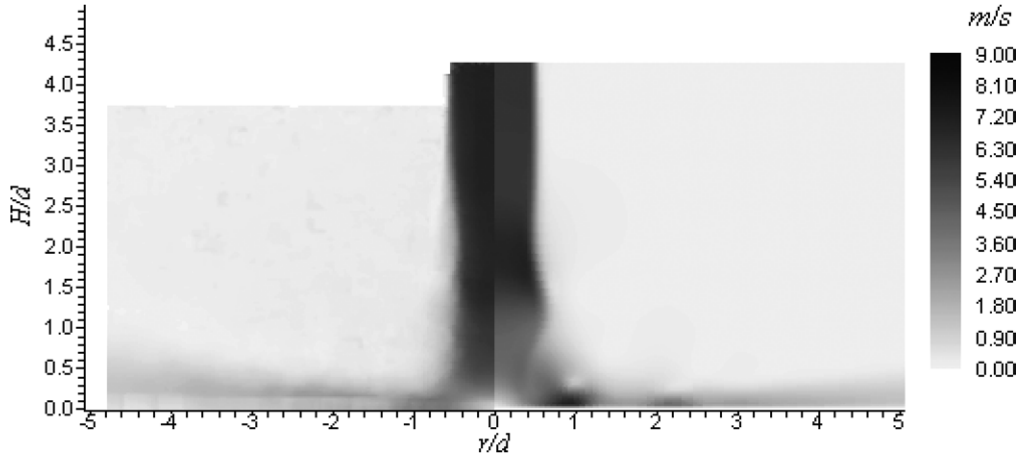

Fig. 6. Comparative PIV (left)/FLUENT^{TM} (right) shaded plots of V. k–ω turbulence model for $H/d = 4.5$: $Re = 4000$.

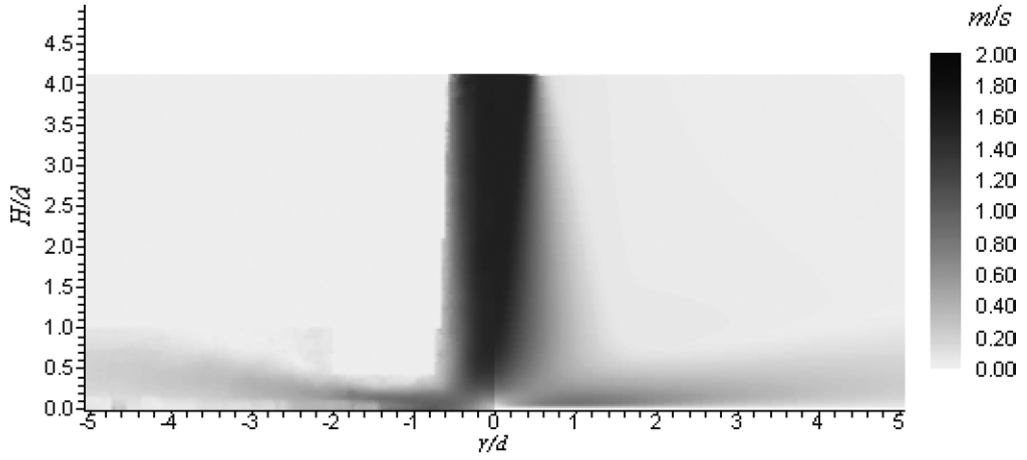

Fig. 7. Comparative PIV (left)/FLUENT^{TM} (right) shaded plots of V. k–ε turbulence model for $H/d = 4.5$: $Re = 1000$.

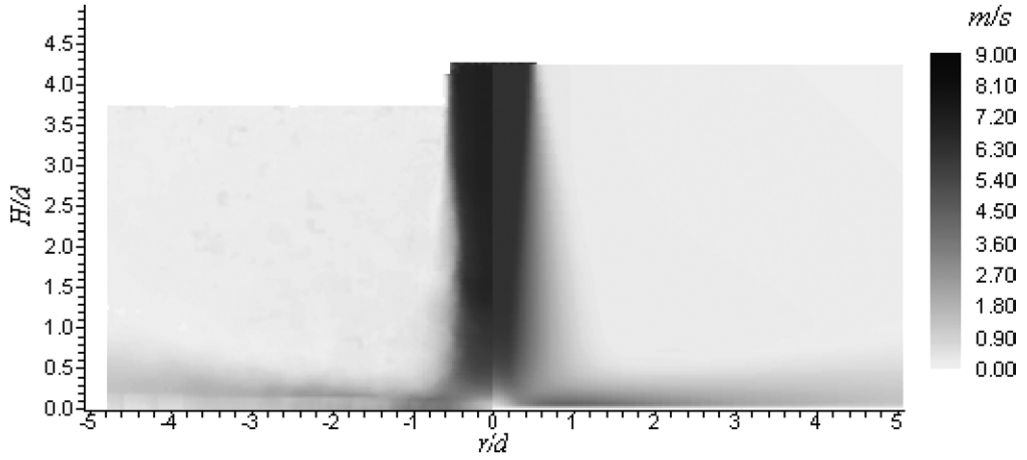

Fig. 8. Comparative PIV (left)/FLUENT^{TM} (right) shaded plots of V. k–ε turbulence model for $H/d = 4.5$: $Re = 4000$.

side) are more visible in the k–ω SST results, which are smoothed down by the k–ε RNG and RSM time-averaging models, as they work by time-averaging the flow variables as well.

In addition to qualitative comparisons, the experimental local Nusselt distributions have also been plotted against the numerical ones (Figs. 12–14), where some of the reported effects of region non-homogeneity is also reflected. These progresses have been already compared to appropriate experimental literature benchmarks elsewhere [3].

All turbulence model appear to perform quite nicely up to $Re = 1500$ in Fig. 12, but starting from $r/d = 2$ the dif-

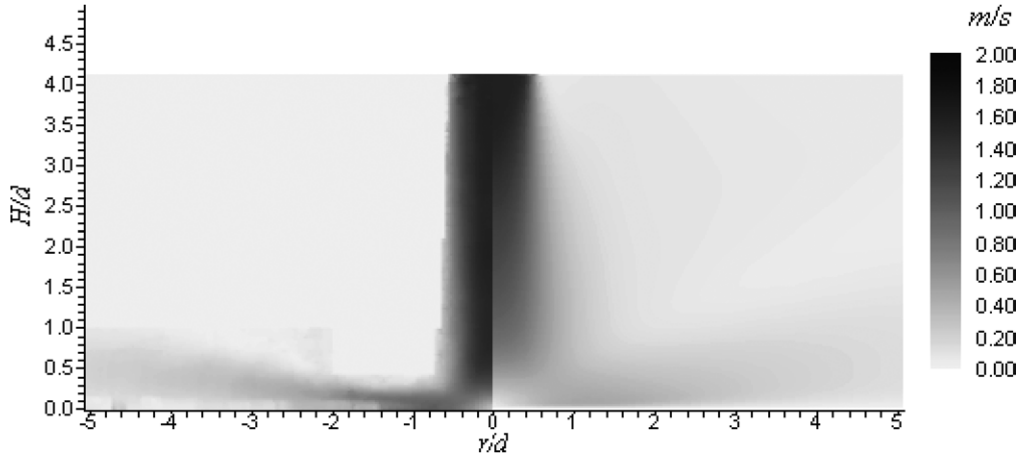

Fig. 9. Comparative PIV (left)/FLUENT^{TM} (right) shaded plots of V. RSM turbulence model for $H/d = 4.5$: $Re = 1000$.

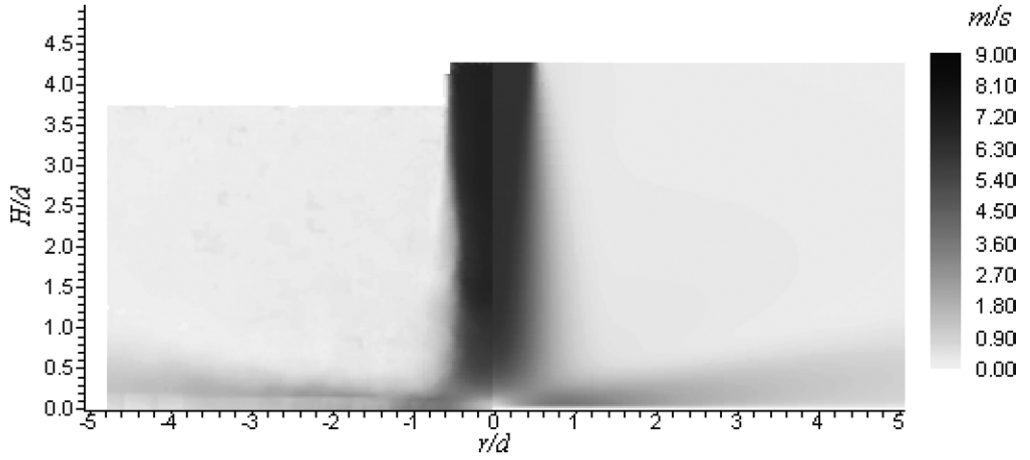

Fig. 10. Comparative PIV (left)/FLUENT^{TM} (right) shaded plots of V. RSM turbulence model for $H/d = 4.5$: $Re = 4000$.

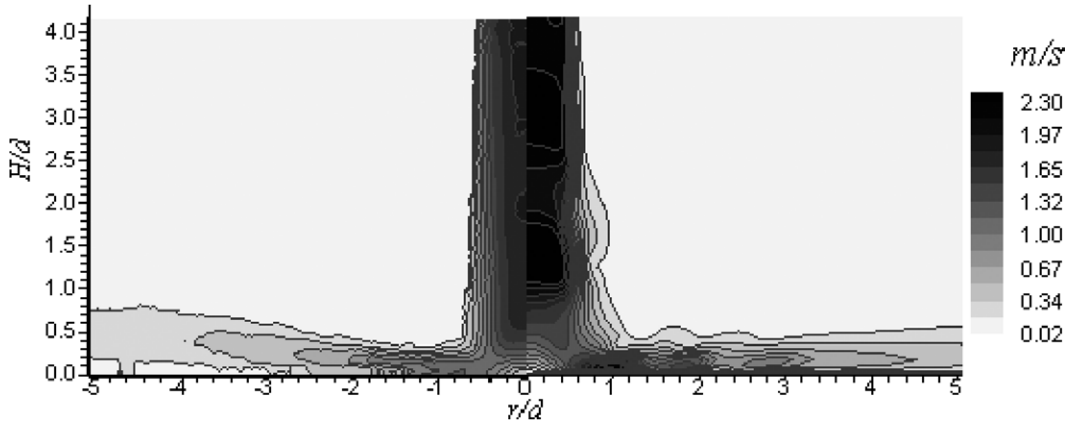

Fig. 11. Quantitative PIV (left)/k–ω turbulence model (right) isocontour plots of V, at $Re = 1000$, for $H/d = 4.5$.

ference with the experimental data is greater than 20%. At $Re = 1000$ the k–ω and RSM models are particularly accurate in capturing the progress within the stagnation region (approximately $r/d \leqslant 0.6$), while the k–ε fails to follow the typical saddle shape. The instantaneous feature of k–ω SST model can still be seen by noting its peculiar, non-monotone progress starting approximately from $r/d = 1.0$. This effect can be attributed to the stationary radial waves or vortices which propagate in the wall jet region's first sector.

At the intermediate $Re = 1500$ in Fig. 13 regime all models seem to under-estimate local heat transfer in the wall jet region, while the RSM model is the best for the saddle shape in the stagnation region.

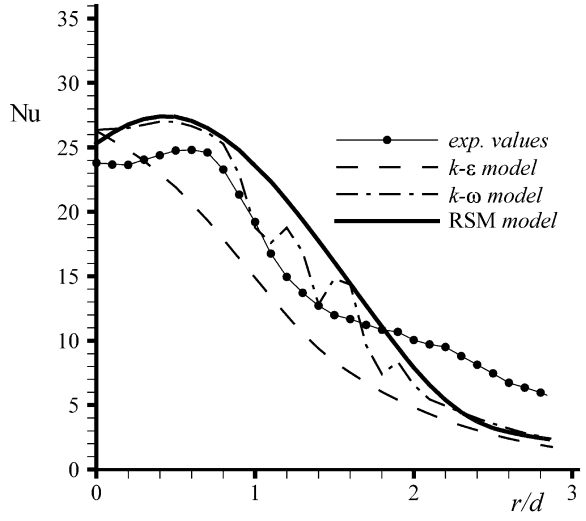

Fig. 12. Local Nusselt number progress for $H/d = 4.5$ at $Re = 1000$.

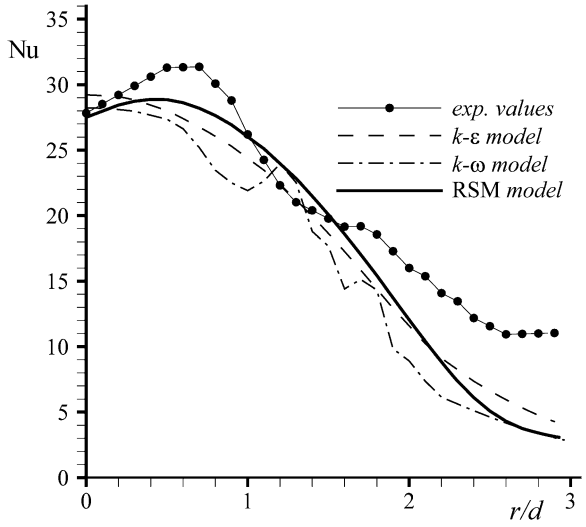

Fig. 13. Local Nusselt number progress for $H/d = 4.5$ at $Re = 1500$.

Finally, for the highest *Re* in Fig. 14, all model fall short in the stagnation region, while for $1.0 \leqslant r/d \leqslant 2.0$ only the k–ε RNG performs adequately and the RSM underestimates the local heat transfer by a 16–25% but following its shape progress.

5. Conclusions

In this paper some configuration of submerged gaseous, transitional impinging jets are numerically and experimentally characterized and compared. A PIV technique has been enforced to extensively investigate on the flow field behavior in the vicinity of the stagnation region, by a high spatial resolution and no intrusively measurements. Nusselt number experimental assessment has been carried out by using the well-known analogy between mass and heat transport. A commercial CFD package has been repeatedly employed to simulate three different configurations, which

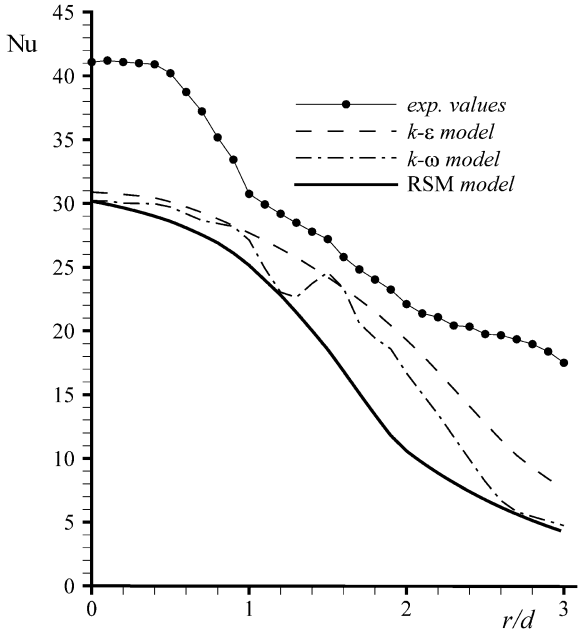

Fig. 14. Local Nusselt number progress for $H/d = 4.5$ at $Re = 4000$.

allowed to validate the different turbulence models, namely k–ε Re-Normalized Group (RNG), k–ω Shear Stress Transport (SST) and the Reynolds Stress Model (RSM). The k–ω SST turbulence model seems more reliable for the investigated configurations, specially at the lower *Re*, for both the flow field and the local *Nu* distribution. For the higher *Re*, the agreement with the experimental data was improved by using k–ε RNG or RSM turbulence models when simulating the flow field, whereas all models where largely inadequate in the heat exchange valuation. These results can be helpful when planning related simulations with the adopted commercial package.

Acknowledgement

This work was funded by MIUR Italian Ministry of Scientific Research, grant no. 2004090750_003 entitled “Analysis of transport phenomena due to jet impingement on substrates in industrial applications”.

References

[1] K. Jambunathan, E. Lai, M.A. Moss, B.L. Button, A review of heat transfer data for single circular jet impingement, Internat. J. Heat Fluid Flow 13 (1992) 106–115.
[2] R. Viskanta, Heat transfer to impinging isothermal gas and flame jets, Experimental Thermal Fluid Sci. 6 (1993) 111–134.
[3] M. Angioletti, R.M. Di Tommaso, E. Nino, G. Ruocco, Simultaneous visualization of flow field and evaluation of local heat transfer by transitional impinging jets, Internat. J. Heat Mass Transfer 46 (2003) 1703–1713.
[4] S. Polat, B. Huang, A.S. Mujumdar, W.J.M. Douglas, Numerical flow and heat transfer under impinging jets: a review, Annual Rev. Numer. Fluid Mech. Heat Transfer 2 (1989) 157–197.

[5] Y.M. Chung, K.H. Luo, N.D. Sandham, Numerical study of momentum and heat transfer in unsteady impinging jets, Internat. J. Heat Fluid Flow 23 (1996) 592–600.
[6] V.A. Chiriac, A. Ortega, A numerical study of the unsteady flow and heat transfer in a transitional confined slot jet impinging on an isothermal surface, Internat. J. Heat Mass Transfer 45 (2003) 1237–1248.
[7] M. Angioletti, Un approccio integrato allo studio dei getti impingenti, Dottorato di Ricerca in “Ingegneria dei Sistemi Termomeccanici”, XV ciclo, 2002.
[8] FLUENT^{TM} 6.0 User’s Guide, FLUENT Inc., 2001.